ELSEVIER

Journal of
Environmental Radioactivity 43 (1999) 31–49

JOURNAL OF
ENVIRONMENTAL
RADIOACTIVITY

Simulation of radionuclide dispersion in the Pacific Ocean from Mururoa atoll

Alban Lazar[a,*], Jacques Rancher[b]

[a] *Laboratoire d'Océanographie Dynamique et de Climatologie, Unité Mixte de Recherche CNRS-ORSTOM-UPMC, Université Pierre et Marie Curie, Paris, France*
[b] *CEA/DAM/DSR/DTDS/SARI, BP 12, 91680 Bruyères-le-Châtel, France*

Received 20 March 1997; accepted 4 April 1998

Abstract

A series of numerical simulations was carried out to evaluate, on a Tropical South Pacific scale, the consequences over 10 yr of radionuclide releases to the ocean from French Polynesian nuclear test sites. Tracer advection and diffusion terms were computed based on a dispersion model using ocean dynamics and turbulent mixing coefficients derived from an Ocean General Circulation Model on the basis of a yearly climatological average. Preliminary experiments demonstrated sensitivity of the results to injection depth and type. Two instant unit releases were then carried out at the model characteristic depths of 5 and 364 m: maximum concentrations decrease by factors of more than 10^4 and 10^3, respectively, over 10 yr. Temporal evolution tables for concentrations are given and can be applied to any given quantity of tracer introduced from Mururoa atoll into the Pacific Ocean. Taken as a whole, our results present, from qualitative and quantitative viewpoints, different dispersion scenarios as a function of release characteristics. Finally, a comparison with the surface release study by Ribbe and Tomczak (1990) shows that, while the order of magnitude of tracer concentrations is comparable, the direction of propagation is significantly different.

1. Introduction

The Mururoa atoll, where France has completed its last series of nuclear tests in deep basaltic formations in 1996, has been described as a potential source of pollution

*Corresponding author. Present adress: Dr. Alban Lazar, Laboratory for Hydrospheric Processes, code 970, NASA/Goddard Space Flight Center, Greenbelt, MD 20771, USA.

0265-931X/99/$ – see front matter
PII: S0265-931X(98)00032-0

to the marine environment (Ribbe & Tomczak, 1990, RT in the following). It therefore seems appropriate to evaluate the impact of such an assumed pollution and to determine its order of magnitude. As a prerequisite, the oceans are influenced by a variety of complex biological, chemical and physical processes, many of which control the transport and most of which are only partially understood. The work described in this paper covers the study of a passive tracer in which biochemical effects are neglected. Furthermore, radioactive decay is disregarded to keep the results applicable to any radionuclide release. The velocities associated with the transport of a substance within a mass of water is low, usually of the order of a few $cm\,s^{-1}$ in the horizontal direction, although it may be as much as one $m\,s^{-1}$ in certain regions. Vertical velocity is even lower, by at least one order of magnitude; a tracer will thus move more slowly in the vertical direction. Further, water masses in the region investigated are divided vertically, from surface to bottom, into three sections of variable thickness: the surface mixed layer down to approximately 100 m, the permanent thermocline about 500 m thick, and the deep ocean. The characteristic strength of currents decreases significantly with depth from one section to the next; the depth at which the tracer is located is thus a key variable directly governing the direction of propagation as well as the signal strength.

The subject of this investigation is the instant release of radionuclides to the marine environment, as a function of depth, using a tracer dispersion model (Marti, 1992) based on yearly averages of climatological fields from an Ocean General Circulation Model (Madec & Imbard, 1993). To obtain data applicable to the largest possible number of dispersion scenarios, we have endeavoured to simulate releases associated with concentration multiplying factors and characteristic directions of propagation. Several simulations of releases from the Mururoa test site in French Polynesia were carried out, and their development over a 10-yr period was investigated. The first step was an instant unit injection over the entire water column. It provided an overall approach to the various propagation scenarios as a function of release depth. In the next experiment, an equivalent quantity was injected, but this time on a continuous basis over a 10-yr period. As compared with continuous, instantaneous release results in increased concentrations far from the source on the South Pacific scale (i.e. a few 1000 km) whereas the maximum activity concentration can always be found in the vicinity of the source for the second case. These two preliminary experiments led us to the study of two unit, instantaneous releases with characteristic directions of propagation and enhanced concentrations compared to other possible dispersion possibilities offered by the model. In a last simulation, we compared the data from a surface release scenario with those from RT.

2. Model characteristics

2.1. The tracer dispersion model

The effects of current and turbulent mixing on a passive tracer were computed with the dispersion model developed by Marti (1992) and used for example by Orr (1993).

The three-dimensional advection-diffusion equation is

$$\partial_t C + \mathbf{U}\cdot\nabla C = \nabla_h\cdot(A\nabla_h C) + \partial_z K\partial_z C,$$

where C is tracer concentration, $\mathbf{U}$ the velocity vector, A the horizontal eddy coefficient and K the vertical eddy coefficient. $\mathbf{U}$ and K are computed from the circulation model, whereas A is isotropic and equal to $2\times10^3\ \mathrm{m^2\,s^{-1}}$. The above equation is solved numerically through an Arakawa scheme as regards the diffusion terms, and through a corrected flux transport scheme as regards the advection terms (Smolarkiewicz & Clark, 1986). In the time-frame of interest (i.e. 10 yr), dimensional analysis shows that, even if tracer path is primarily determined by advection terms, diffusion is still an important factor. Over a 10-yr period T, the displacement range due to horizontal diffusion is of the order of 800 km ($\sqrt{A\times T}$) whereas the displacement due to advection exceeds 3000 km in the thermocline ($U\times t$, $U\approx 1\ \mathrm{cm\,s^{-1}}$). In the upper first kilometer, the incidence of currents on the distance covered therefore exceeds that of diffusion by an approximate factor of 4.

2.2. The oceanic circulation model

The velocity and diffusion fields used in the above series of experiments were abstracted, on a yearly average basis, from a worldwide climatological year simulated by an OGCM in forced mode using primitive equations (Delecluse et al., 1993). A presentation of the model and some of its results can be found in the studies of Madec and Imbard (1996) for the forced mode and of Guilyardi and Madec (1997) for the coupled mode. This type of model allows direct comparison with the ocean since it solves the dynamic equations for geophysical fluids while associating internal variables and surface fluxes with climatological fields. Horizontal resolution in the South Pacific is two degrees of longitude and 0.5–1.7° of latitude. There are 30 vertical levels, including 16 in the top 200 m. The vertical diffusion coefficient is computed on the basis of a turbulent closure (Blanke & Delecluse, 1993) and depends thus on geographical location and depth. The wind forcing is computed from the Hellerman and Rosenstein (1983) atlas. The heat Q and freshwater E surface fluxes are given by expressions:

$$Q = Q_{\mathrm{Esb}} - \left.\frac{\mathrm{d}Q}{\mathrm{d}T}\right|_{c\,\mathrm{lim}}(T - T_{\mathrm{Lev}}) \quad\text{and}\quad E = E_{\mathrm{Obe}} - \left.\frac{\mathrm{d}E}{\mathrm{d}T}\right|_{c\,\mathrm{lim}}\frac{S - S_{\mathrm{Lev}}}{S},$$

where Q_{Esb} and E_{Obe} are the net heat and freshwater flux computed from the Esbensen and Kushnir (1981) and Oberhuber (1988) climatology respectively, T_{Lev} and S_{Lev} are interpolated from the Levitus (1982) data, the coefficients $(\mathrm{d}Q/\mathrm{d}T)|_{c\mathrm{lim}}$ and $(\mathrm{d}E/\mathrm{d}T)_{c\,\mathrm{lim}}$ correspond to a restoring time-scale of ten days over the first ten meter depth. Below the surface, the temperature and salinity fields are restored to the Levitus (1982) data and a penetrating solar radiation scheme is used.

2.3. Simulation configuration

This study covers the dispersion of a tracer from Mururoa atoll, in the Tuamotu Archipelago, into the South Pacific over a 10-yr period. By using dynamic fields

extending over a single climatological year, we are clearly disregarding the inter-annual variability of the tropical Pacific, affected as it is by the Austral Oscillation (Philander, 1990) among other phenomena. Further, we have limited ourselves to the yearly average of the dynamic fields, thus eliminating part of the non-linear advective and diffusive terms. We therefore feel that our data represent a zero-order approximation as regards oceanic circulation in the South Pacific. The method requires no excessive amount of computing time, while accounting for the major structures of general circulation, which is one reason for adopting it. The most rigorous use of the tracer model to investigate dispersion through the ocean would require consideration of the global ocean dynamic field. The computing cost of such a study would be excessive, due to the short time steps required to resolve the strong equatorial currents as well as to the number of meshes to be processed. We must therefore restrict the range of our investigations to a sub-area centered on Mururoa atoll at 21°50′S, 138°52′W (Fig. 1), with a mesh pattern identical to that of the oceanic circulation model. The handling of the boundaries open to the ocean then presents a numerical problem. We have elected to arbitrarily hold the tracer concentration at zero beyond these boundaries. This technique introduces two types of error into the model: there is excessive diffusion towards the zero-concentration area, and a quantity of tracer exiting the investigated area will be unable to return by advection. Therefore, these two effects will cause an underestimation error in the concentration to a varying degree in each experiment but, as developed later, our results show that its maximum is well below a factor of 2. Thus this error does not affect the order of magnitude of the concentrations, which is consistent with the aims of our study. Finally, the initial tracer concentration in our ocean model is assumed to be zero, since we have chosen to disregard the radionuclide concentrations existing worldwide in the ocean (i.e. the background noise). The following analysis is based on instantaneous tracer concentration fields derived at the end of each year.

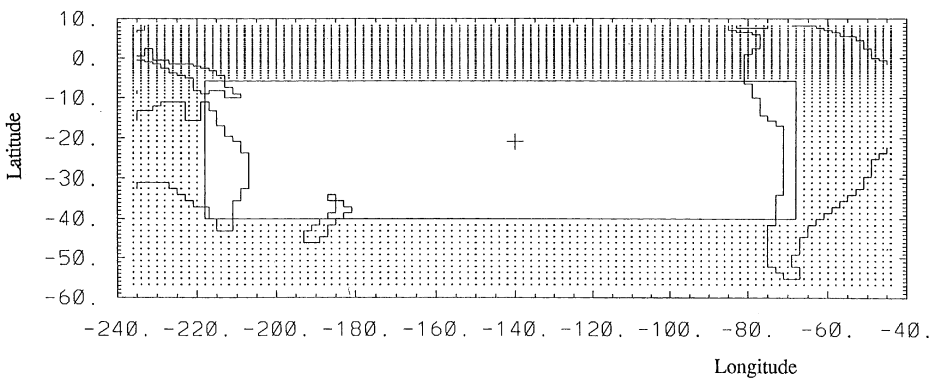

Fig. 1. Area covered by the tracer dispersion model, Mururoa atoll is shown by a cross (longitudes −240, −220 and −200 correspond to 120, 140 and 160° East, respectively).

2.4. Simulated ocean dynamics

Current simulations highlight at three major structures as a function of depth in the central region of the South Pacific (Fig. 2); these structures affect tracer dispersion in different ways. The surface structure is related to the sub-tropical anticyclonic gyre, centered around 20°S in the eastern zone of the basin (Fig. 2a). Comparing surface currents with the averaged measurement data collected by Reverdin et al. (1994) over the entire equatorial Pacific area (in the top 15 m) shows the model to be representative of the direction and magnitude of the velocity vectors in this large-scale dynamic structure. The gyre extends from the equator to 40°S. Its northern branch, moving west, shifts to the south as depth increases, becoming predominant over the southern branch which moves east. The gyre roughly occupies the top 400 m. On the surface, Mururoa is located between the two branches, with currents tending to be along the

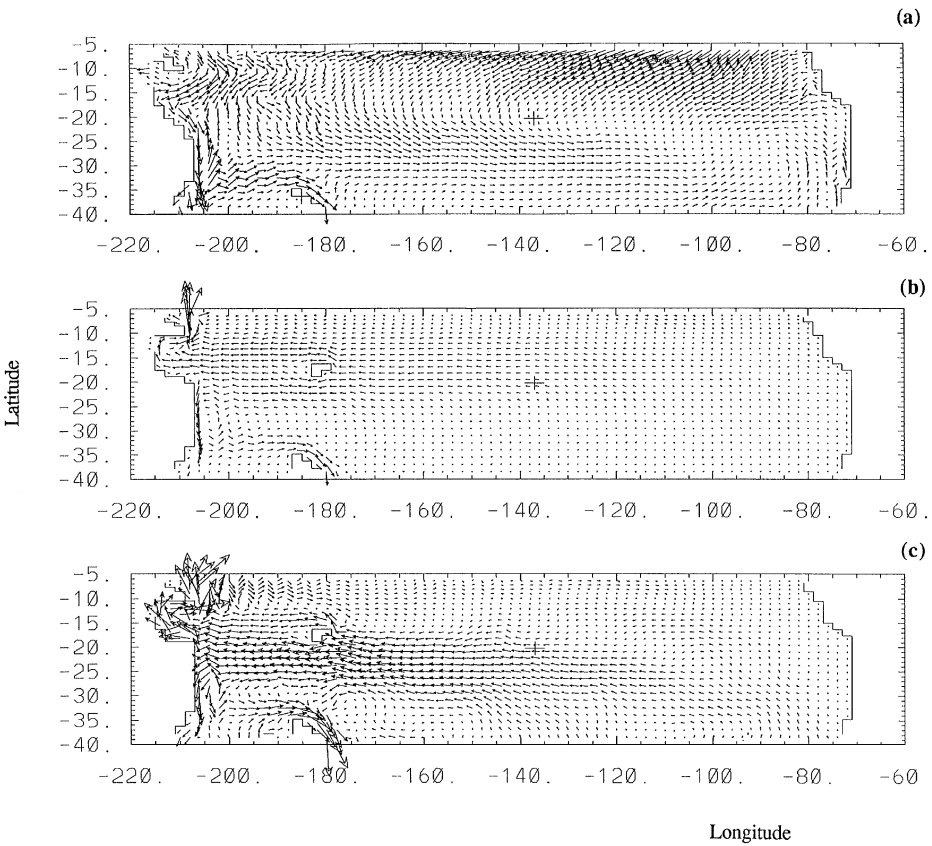

Fig. 2. Horizontal current fields at various depths in the model, showing (a) at 25 m, the sub-tropical gyre (1 mm = 3 cm s^{-1}), (b) at 364 m, a large zonal current moving westwards (1 mm = 2.5 cm s^{-1}), (c) at 732 m, Intermediate Antarctic Water flowing from S–E to N–W (1 mm = 0.6 cm s^{-1}).

meridian and oriented towards the south branch, which will thus be predominant in tracer advection. In the top 50 m, current mean velocity reaches 5 cm s^{-1}. Further below, the northern branch current is reaching Polynesia and, at a depth of 364 m (Fig. 2b), the velocity is of the order of 2 cm s^{-1} towards the west. The second major structure is found roughly between 500 and 1500 m: this is the Intermediate Antarctic Water (IAW), flowing from east to west, with a slight bend to the north-west which increases with depth. Velocity is of the order of 1 cm s^{-1}. Below 1500 m,

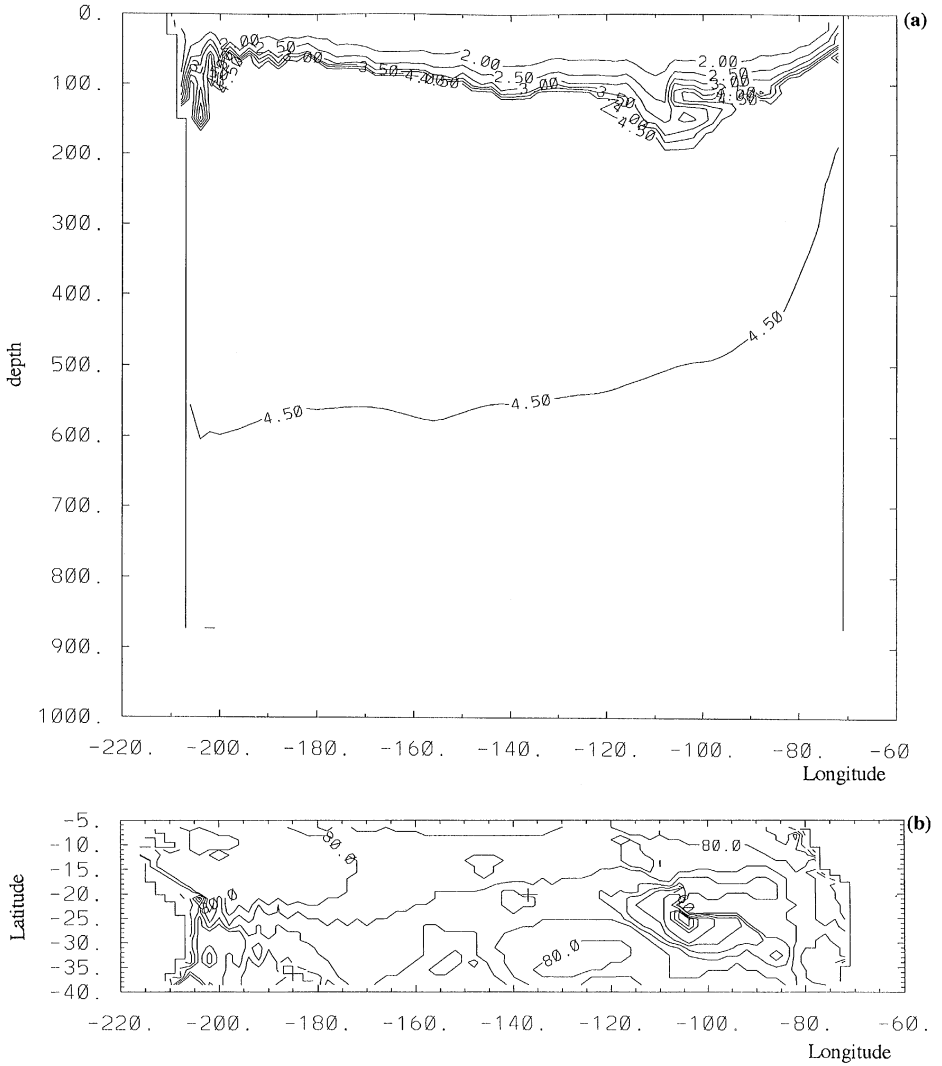

Fig. 3. (a) Vertical profile of $-\log_{10} K$ (K in $m^2 s^{-1}$) at 21°S, contour interval = 0.5 and (b) depth of the mixed layer (as determined by values of K in excess of 5×10^{-5} $m^2 s^{-1}$), contour interval 20 m.

a smaller-scale gyre structure can be observed. With no real uniformity, it is influenced by topography and the velocity is of the order of 1 mm s^{-1}. When simulating tracer dispersion, the dynamic effects unresolved by the circulation model (i.e. the dynamics with characteristic length smaller than the mesh size and a time-scale smaller than the time step) are parameterized by a turbulent diffusion term proportional to tracer gradients, with a constant horizontal diffusion coefficient and a space-dependent vertical diffusion coefficient K. The horizontal turbulent mixing thus depends on local concentration only, while the vertical turbulent mixing depends, for a given concentration gradient, on depth and geographical location. It should be noted that, in the basin considered, values of K along the vertical are subject to three different patterns. Plotting this coefficient against depth at latitude 21°S (Fig. 3a) shows it to be highest close to the surface (100 cm^2 s^{-1} where a strong vertical mixing is induced mainly by wind stress conditions). The mixed layer extends from the surface to a depth which can be as much as 240 m in the eastern part of the basin (Fig. 3b). Further down, the coefficient assumes its minimum values (from 0.1 to 1 cm^2 s^{-1}). It then rises gradually with depth (following the inverse Brunt-Väsälä frequency), while remaining several orders of magnitude below its value in the mixed layer. If released into the mixed layer, a tracer will be homogenised from the surface to the bottom of that layer and its concentration will therefore drop much more sharply than if it had been released lower down.

3. Results

3.1. Instantaneous release to entire water column

A tracer with 1 Bq m^{-3} concentration was injected at the initial time step into the entire water column at the geographical position of Mururoa atoll. The presence of tracer throughout the depth range precludes the accurate quantitative analysis of an emission at any given depth: diffusion effects are strongly attenuated due to the presence of tracer introduced into the upper and lower layers. The concentrations measured are thus higher than those observed following release at a given depth. In contrast, since advection remains unchanged, one obtains a good qualitative appreciation of the predominant directions, on a yearly average basis, of large-scale transport as a function of depth. Tracer column dispersion is analysed from the surface down to an approximate depth of 200 m, then from 200 to 800 m and below 800 m.

In the top 100 m, a spot forms and, in the first few years, moves away from the rest of the tracer at the bottom of the mixed layer. It moves to the southeast under the influence of the southern branch of the sub-tropical gyre. Its velocity in the horizontal plane is high, in the order of 5 cm s^{-1}, the direct consequence being a strong diffusion all along the path. Since the tracer moves rapidly towards the regions in the basin where concentration is nil, concentration gradients remain strong, actively promoting diffusion in the horizontal and vertical directions. As early as the first year, the strong vertical homogenisation which takes place in the mixed layer results in an almost uniform distribution of the tracer from the surface down to about 100 m; however,

a concentration peak appears at the surface, moving deeper with time. Dilution is maximum, with a factor of 300 as compared with the other parts of the column. After 5 yr, the concentration peak is found at a depth of 100 m, its approximate position being 120°W –24°S (Fig. 4a); carried by the northern branch of the sub-tropical gyre, it starts on a return loop towards the north-west. It sinks deeper and moves under the

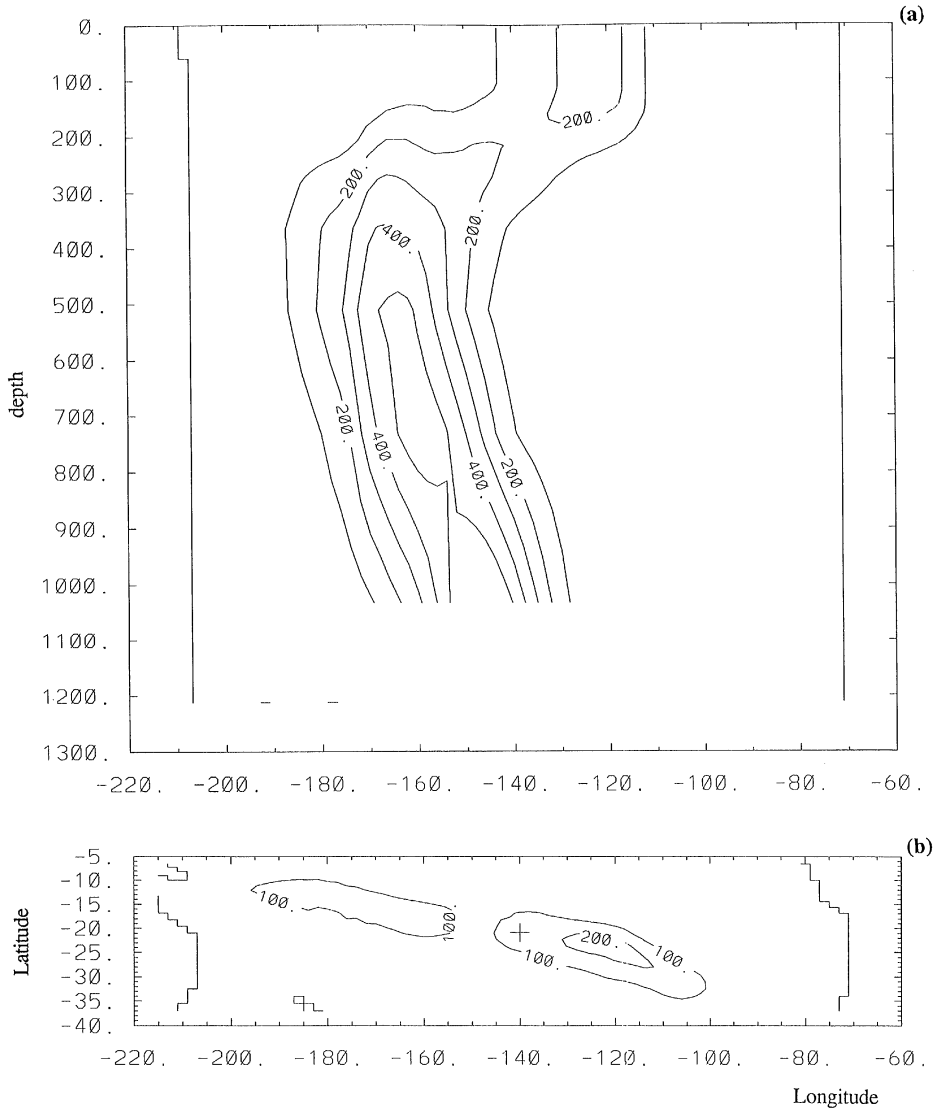

Fig. 4. Column-type instantaneous release. Tracer concentration after 5 years, contours are $100_1 \times {}^{1}0^{-5}$ Bq m^{-3} intervals. (a) Vertical/zonal profile at 24°S, from surface down to 1000 m. (b) Horizontal field at 106 m depth.

mixed layer. After 10 yr, it is located at an approximate depth of 180 m, slightly northwest of its 5-yr position. From a depth of 50 m, the northern branch of the sub-tropical gyre, moving west, begins to flow into the Polynesian region, while the effects of the eastwards current are less noticeable. This results in a split of the column, between 50 and 200 m depth, as early as the first year. Figure 4b shows the horizontal concentration field at a depth of 106 m after 5 yr. The tracer injected in that depth range divides into two streams, one moving to the south-east and the other to the northwest, respectively representing the base of the surface spot and the top of the lower column.

Between 200 and 800 m depth, tracer advection is westwards, due to a zonal current which covers the whole northern half of the region investigated. A concentration peak appears between 350 and 500 m during the second year, moving west at a constant depth. Fig. 5 partly shows the vertical and horizontal spread of the column after 8 yr. A meridian cross-section at 17°S (Fig. 5a) shows a pronounced westwards tilt caused by a decrease in velocity with depth. The geographical position of the core is shown in Fig. 5b at 364 m. After 9 yr, the peak tracer concentration has reached the longitude of the Australian and Indonesian coastlines at 16°S. Throughout the experiment, the concentration peak dilution was 7 times lower than the column top dilution. Thus, the joint effects of advection and diffusion are more conservative with respect to deep-water concentration than at the surface; there are two reasons for this. First, the tracer spot core moves through a region of low current velocity and shear; concentration gradients are thus reduced in comparison with the surface, and horizontal diffusion less active. Second, since the vertical diffusion coefficient nears its minimum value at that depth, the associated diffusion is low. Deeper down, towards 700 m, the column moves slowly westwards, covering 3000 km in 8 yr (Fig. 5c). At this stage, the tracer core concentration is comparable to that at the 364 m level, and the core is located at approximately 170°W, at the Mururoa latitude.

Below 800 m, diffusion and meso-scale gyre circulation scatter the tracer, slowly and more or less uniformly, around the release points. Within our 10 yr time-frame, we may thus consider that the column is practically at a standstill, and that the maximum concentration remains located off Mururoa.

The above experiment therefore yields two dispersion patterns, characteristic of a simulation on a yearly average basis, following instantaneous release: one eastwards starting at 5 m depth, maximizing concentrations from the surface to a depth of 100–200 m; the other westwards, from 364 m depth, maximizing concentrations in the 100–200/800 m range.

3.2. Continuous release throughout the water column

Another column-type simulation was carried out, this time assuming the continuous release of the same tracer quantity over a 10-yr period, the release being of the order of 100 $Bq\,s^{-1}\,m^{-1}$ depth at the same geographical location as before. Fig. 6 shows the horizontal concentration fields after 10 yr, on the surface and at 364 m depth. Throughout the 10-yr period, the maximum concentration occurs at source level because of the continuous influx. On a regional scale, values are higher than for

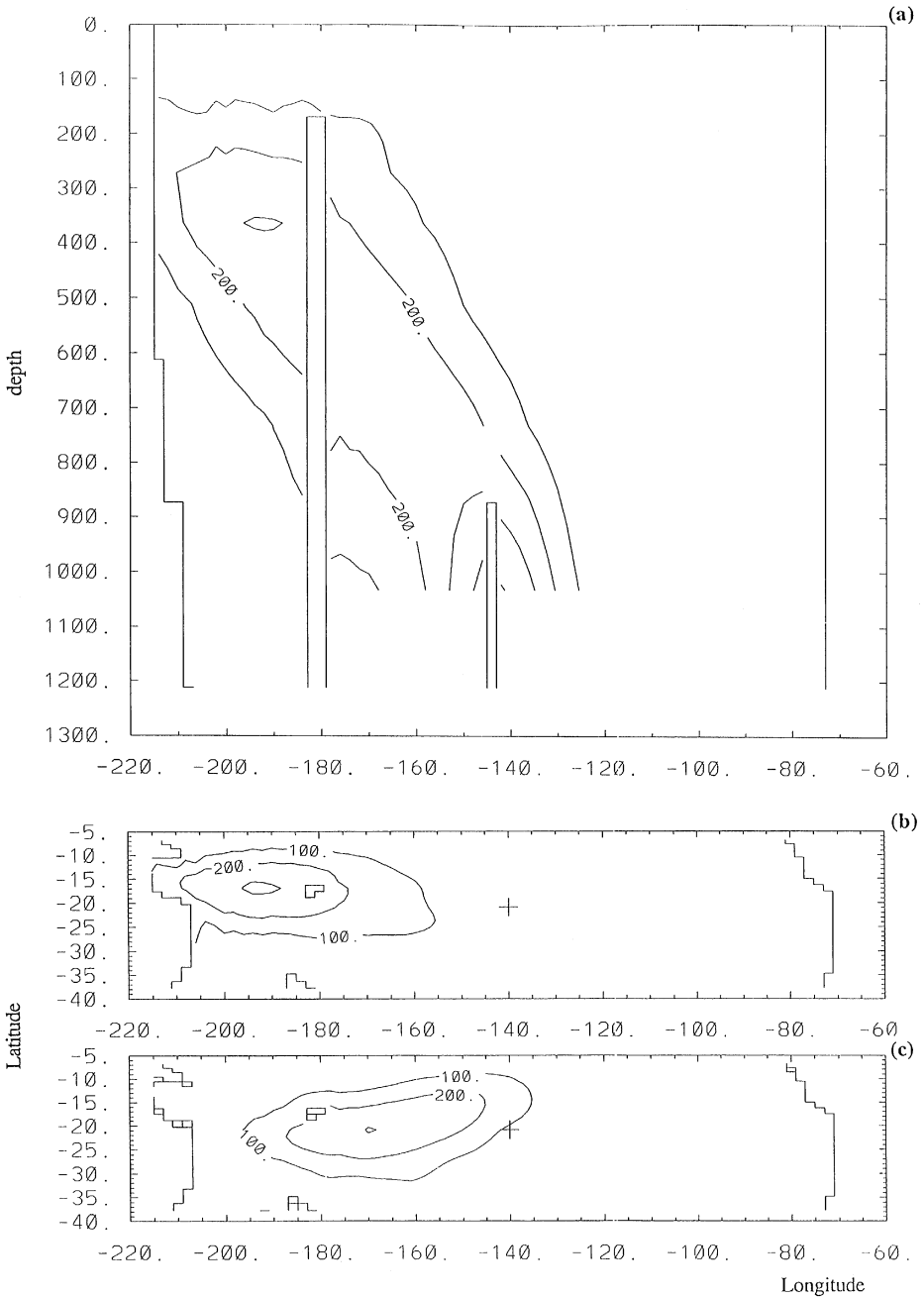

Fig. 5. Column-type instantaneous release. Tracer concentration after 8 years, contours are 100×10^{-5} Bq m^{-3} intervals. (a) Vertical profile at 17°S from surface down to 1000 m. (b) Horizontal field at 364 m depth. (c) Horizontal field at 732 m depth.

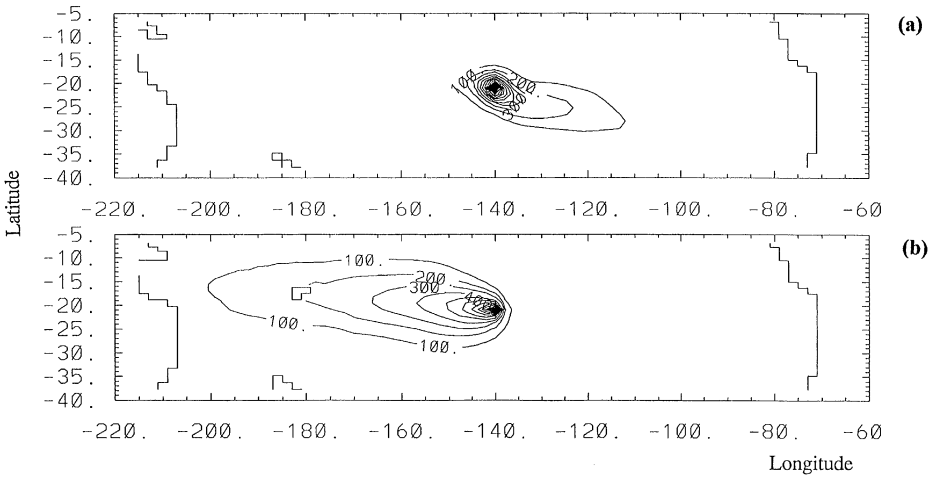

Fig. 6. Column-type continuous release. Tracer concentration after 10 years, contour interval = 100×10^{-5} Bq m^{-3}. Horizontal field at (a) 5 m depth, (b) 364 m depth.

an instantaneous release but, at significant distances of the order of 1000 km, the instantaneous injection produces higher concentrations. It seems therefore that, for a study carried out over more than 10 yr, it is the continuous release that would result in maximum concentrations. On the basis of the above results and considering our time-scale of one decade, we can now restrict our investigations to the simulation of instantaneous releases, which lead to the highest concentrations and hence to the most conservative assessments.

3.3. *Instantaneous release at the surface*

In this simulation case, a tracer with unit concentration is introduced, at a depth of 5 m, in a volume element of 3.19×10^{11} m^3 of 10 m thickness (the released activity is thus 3.19×10^{11} Bq). The tracer spot moves along the same path (Fig. 7) as the surface release did in the column simulation. Although eastwards motion predominates, one observes westwards dispersion due to the currents in the northern branch of the sub-tropical gyre. Current shear causes the spot to stretch along the south-east/northwest axis. Table 1 shows concentration peak characteristics obtained in the area of interest as a function of time. At the end of the time period, the loss of tracer through open boundaries reaches 30% of the initial quantity. This loss occurred progressively with time but mainly in the second half of the period when the tracer core was closer to the boundaries. A part of this loss is due to excessive diffusion and the absence of inwards transport, both related to the artificial open boundary conditions, but the rest comes from realistic outwards advection and diffusion through the open boundaries, and it is certainly significant. These 30% represent roughly half of the total quantity remaining after the 10-yr period which means that,

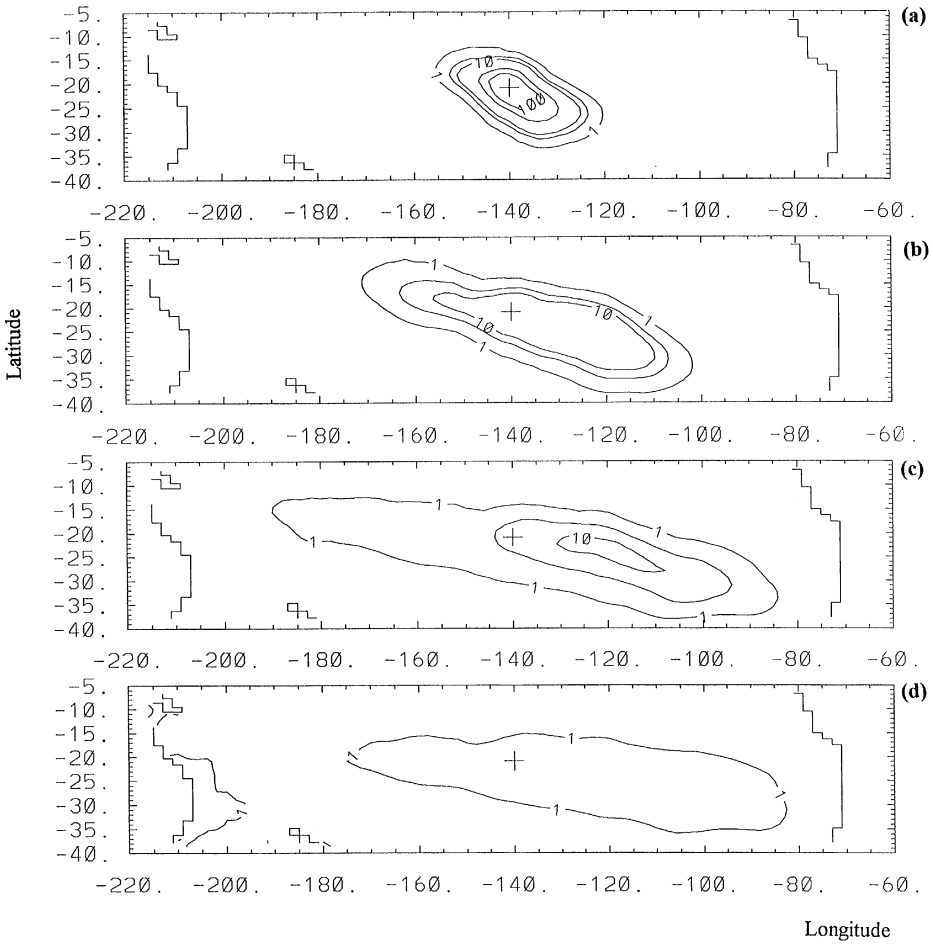

Fig. 7. Instantaneous release at 5 m depth. Horizontal tracer concentration fields at 5 m, contours at 1, 5, 10, 50, 100 ($\times 10^{-5}$ Bq m^{-3}). (a) After 1 yr, (b) after 3 yr, (c) after 6 yr and (d) after 9 yr.

even if there was no artificial loss through the open boundary, the concentration in the core at this time would not exceed the shown concentration by more than half. Therefore the order of magnitude of the concentrations predicted here is reliable. Due to the linearity of the tracer model, one can use this table to compute the highest concentrations following any given tracer quantity release between the surface and 100–200 m depth. Concentration is typically ten times less than in the 'column' release. This difference is explained by the fact that vertical diffusion is no longer attenuated by the presence of tracer in the top and bottom adjacent layers; dilution is therefore much quicker. After the first year, due to the strong vertical diffusion which characterises the mixed layer, the maximum concentration has dropped sharply and the tracer distribution is, in effect, quasi-homogeneous throughout the layer depth for

Table 1
Concentration peak characteristics after the surface injection as a function of time

Time (yr)	Longitude (°W)	Latitude (°S)	Depth (m)	Concentration ($Bq\,m^{-3}$)
0	140	21	5	1
1	140	21	95	23×10^{-4}
2	138	22	5	$7{\cdot}4 \times 10^{-4}$
3	124	25	5	$3{\cdot}8 \times 10^{-4}$
4	120	25	5	$2{\cdot}4 \times 10^{-4}$
5	118	25	5	$1{\cdot}5 \times 10^{-4}$
6	120	24	5	1×10^{-4}
7	118	24	65	$0{\cdot}7 \times 10^{-4}$
8	128	21	142	$0{\cdot}5 \times 10^{-4}$
9	216	10	5	$0{\cdot}7 \times 10^{-4}$
10	216	10	5	$0{\cdot}9 \times 10^{-4}$

the entire duration of the simulation. A concentration peak can be seen to occur as a function of time, sinking gradually to a depth of 142 m over 8 years. The sinking is limited to the mixed layer during the first 7 yr. Later, at the approximate position 125°W–22°S, the core of the spot goes under the mixed layer. After 9 yr, the maximum concentration in the basin is again on the surface, but this time in the westernmost part, between Australia and New Guinea. This remote location reflects the gradual tracer dispersion on the surface along the northwest/southeast propagation axis. Thus, the maximum concentration after 10 yr is more than 10^4 times less than the initial concentration, and is approximately the same in the northwest and in the southeast of the area considered.

3.4. Instantaneous release to the thermocline

The second injection with 1 $Bq\,m^{-3}$ concentration was carried out at a depth of 364 m. The quantity released (3.7×10^{12} Bq) was about 10 times larger than before, being commensurate with the size of the volume element, now 116 m thick. As in the 'column' experiment, the spot moves along with the westwards current (Fig. 8), while undergoing diffusion in an approximately circular pattern, since at that depth there is little current shear to distort it. Table 2 shows peak concentration data in the area of interest as a function of time. The loss of tracer out of the domain at the end of the 10-yr period reaches roughly the same percentage of the remaining total quantity as before. The underestimation error on the concentration at the end of the time period which is due to open boundary conditions is thus again much less than half the value shown. Therefore, the order of magnitude of the concentrations is reliable. The table can now be used to derive the highest concentrations following a tracer release between 100–200 and 800 m. The peak moves at a practically constant depth, since vertical currents are very weak. Concentrations are at least ten times higher than in

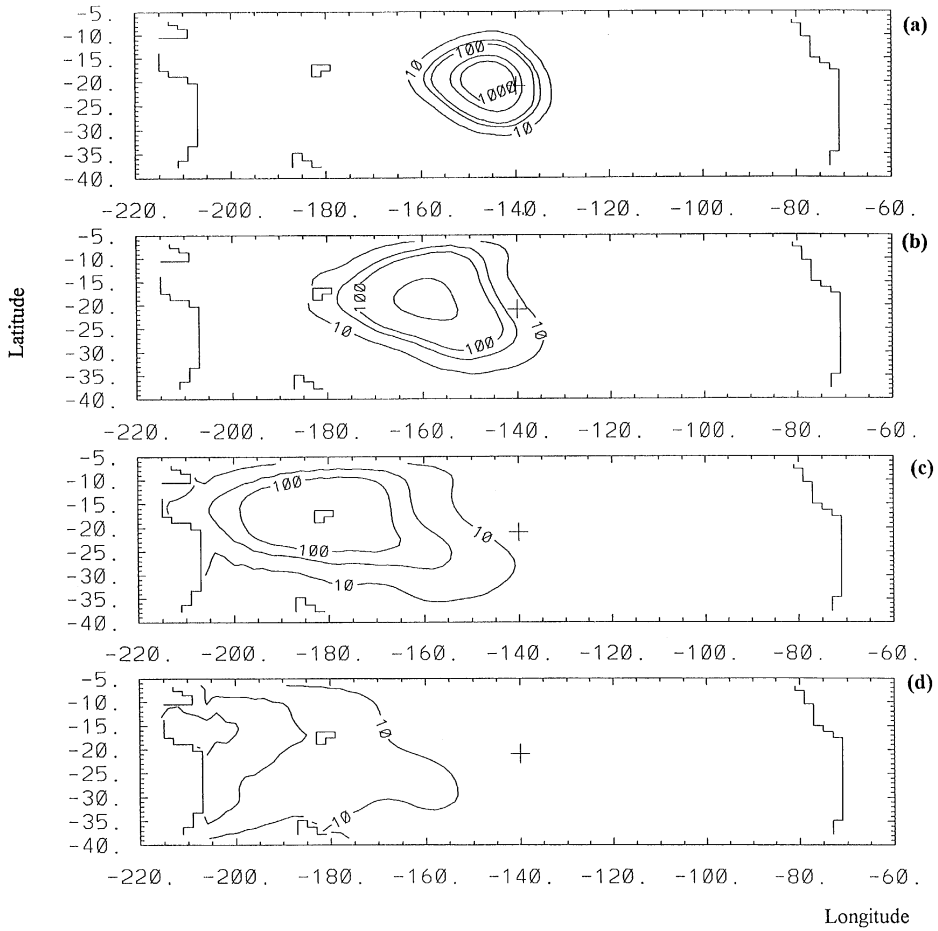

Fig. 8. Instantaneous release at 364 m depth. Horizontal tracer concentration fields at 364 m depth, equal concentration lines at 10, 50, 100, 500, 1000 ($\times 10^{-5}$ Bq m^{-3}). (a) After 1 yr, (b) after 3 yr, (c) after 6 yr and (d) after 9 yr.

the surface release case practically throughout the entire period. This is due mainly to the low current velocities, and less to the low degree of vertical diffusion at that depth. The core of the spot has covered close to 5000 km over 9 yr at an average velocity of 1.5 cm s^{-1}; at that point, it nears an open boundary, which should cause its concentration to be slightly underestimated. From the ninth year to the tenth, the core is seen to move quickly south by 7° of latitude. This is explained by the arrival of the spot, at that time, close to Australia at a latitude (15°S) where the westwards current splits into two streams which accelerate towards the south and north along the coastline. Over 10 yr, the maximum concentration has decreased by a factor of 1000.

Table 2
Concentration peak characteristics after the 364 m depth injection as a function of time

Time (yr)	Longitude (°W)	Latitude (°S)	Depth (m)	Concentration ($Bq\,m^{-3}$)
0	140	21	364	1
1	146	20	364	292×10^{-4}
2	152	20	364	130×10^{-4}
3	160	18	364	75×10^{-4}
4	166	18	364	51×10^{-4}
5	174	17	364	36×10^{-4}
6	180	18	364	27×10^{-4}
7	190	16	364	20×10^{-4}
8	200	16	364	16×10^{-4}
9	212	18	364	12×10^{-4}
10	210	11	364	10×10^{-4}

3.5. Comparison with the Ribbe and Tomczak (1990) study

To compare our simulation data with those of RT, we assumed the instantaneous release of 3.2×10^{17} Bq at 5 m depth as in their study. RT resolved the dispersion equation through a different numerical scheme, whereas the dynamic fields, on a yearly climatological average basis, were derived from a coupled ocean–atmosphere model (Manabe & Stouffer, 1988). Their simulation is characterised by a westwards advection of the tracer peak. This result is in disagreement with ours, since we observe a motion in the opposite direction, i.e. eastwards. This suggests significant differences between the current fields in the first depth levels in our simulation and in RT. The reason may be found in the differences in the atmospheric forcing, and perhaps also in the different vertical resolutions of the two models. The latter assumption was tested by taking the vertical average of the currents in the first five levels of our model to obtain a surface resolution identical to RT's (their first level is 50 m thick). It can be seen that velocity remains oriented in an easterly direction. The discrepancy in results is thus only accounted for by differences in surface forcing between our model in forced mode and the RT ocean-atmosphere coupled model. Considering that the tracer released on the surface is transported by currents which are strongly wind-driven, it is reasonable to think that this difference in direction is due in large part to differences in wind forcing. Indeed, our OGCM is forced by the climatological field of Hellerman and Rosenstein (1983) while the ocean model used by RT is coupled to an atmospheric model in which wind is a prognostic variable. The flow patterns are also controlled by surface heat and salt fluxes which can differ significantly if they are based on a restoring formulation like ours or calculated by more complex air-ocean interactions equations as in the atmosphere model used by RT.

We then compared temporal changes in concentration peaks as given by the tracer dispersion models. RT use a Monte Carlo technique to compute the dispersion of the

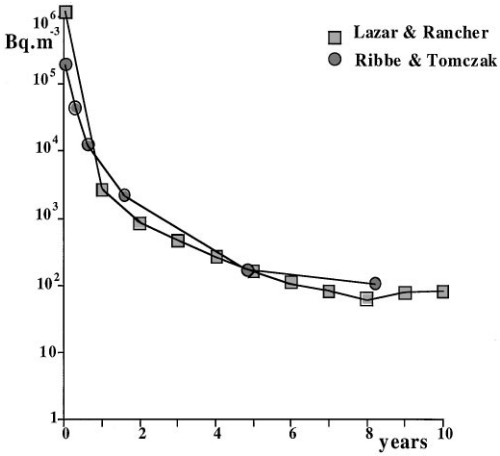

Fig. 9. Peak concentration changes with time in the area investigated, as determined by the Ribbe and Tomczak experiment and our own.

tracer. This method presents the advantage of avoiding numerical diffusion which is on the contrary associated with the classical laplacian diffusion scheme we used. Meanwhile, the artificial numerical diffusion experienced in our simulation will have a negligible role on the discrepancy between the two studies because of the much more significant impact of the very different diffusion coefficients. Our horizontal diffusion coefficient is twice as high as that used by RT and the turbulent closure scheme computation raises the vertical diffusion coefficient in the surface layers by a factor which may be as much as 100 in some places. In contrast, RT have simulated radioactive decay, in this case that of ^{137}Cs with 30.15-yr half-life. Further differences are those originating from advection and shear effects since the spots move in opposite directions. However, current and shear data for the first 50 m of depth are comparable for both paths, at least during the first part of the decade. Fig. 9 shows the changes with time in peak concentration in our experiment and RT's. It should be noted that the initial concentrations, which are based on identical tracer quantities, are not equal in view of the differences between the volume elements in the models. After the first year, the concentrations in our experiment are lower by a factor of one to three; the orders of magnitude, however, are comparable. In fact, the main reason for the difference is the stronger vertical diffusion in the mixed layer due to the much higher vertical mixing coefficient computed by the turbulent closure scheme.

4. Discussion

These simulations provide a better understanding of the consequences of a passive radioactive tracer release from Mururoa atoll, quantitatively through the concentration figures and qualitatively by monitoring the geographical location of the spot

cores. Our simulations show spot displacement to be strongly dependent on depth. On the surface, in the top 100–200 m, the core moves towards the southeast, sinking gradually at the same time; its concentration is reduced by a factor of more than 10^4 in 10 yr. It does not reach the South American coastline, since it follows the sub-tropical gyre's rotary motion, moving rapidly towards the north-west. When injected deeper down to approximately 800 m, the core moves west at constant depth. For a near 350 m depth release, it finally reaches the Australian coastline after 9 yr, with a concentration approximately 10^3 times lower than the initial value. Deeper down, below 800 m, tracer motion is no longer significant in the time-frame considered.

The above results reflect some of the limitations of our numerical tool. As regards the tracer model, a better quantitative assessment of the incidence of open boundary conditions would allow an increase in the precision of the estimates of concentrations, which is here limited by an underestimation by between 0 and 50%. Moving the open boundaries away from the path of the tracer spot core would improve the simulation, particularly in the western part of the basin for the last years. As to the dynamic model, the scope of our work is limited by a low space-time resolution and by the lack of sophistication of the surface forcing. First, a finer mesh structure would permit simulation of a whole range of phenomena which might change tracer dispersion. In particular, some of the turbulent dynamics could be computed explicitly instead of being parameterized through an isotropic horizontal diffusion factor which tends to make the tracer spot too circular in shape. However, on a Pacific-wide scale over 10 yr, we may regard the diffusion terms as representing the mean effect of physical phenomena which remain to be analysed. Second, release simulation on the basis of monthly ocean dynamic fields, instead of yearly averages, would make it possible to fully consider the advection and vertical diffusion terms (whereas part of those are eliminated by time averaging). We could then simulate the passage of oceanic wave fronts, winter baroclinic activity or strong seasonal phenomena such as the convection-induced submergence of surface water during the summertime evaporation peaks. These phenomena could affect tracer penetration depth and therefore the direction of tracer propagation. Third, it should be remembered that fluctuations in Pacific Ocean conditions throughout the year have been disregarded, since the ocean dynamic fields used covered a single climatological year. Still, the El Niño Southern Oscillation, for example, is capable of causing the reversal of certain currents and altering atmospheric circulation for several months. It would thus be worthwhile to introduce variability on a 10 yr scale through the use of ocean dynamic fields generated by a number of distinct simulations. In the same way, and since the South Pacific remains an area about which data are scarce, the sensitivity of the results to impressed atmospheric conditions will be open to investigation, on the basis of ocean dynamics influenced by a variety of atmospheric fluxes derived from measurements or models.

The comparison with the Ribbe and Tomczak (1990) study of a ^{137}Cs surface release is instructive. The two investigations show the core of the spot travelling in opposite directions. One of the reviewers suggested that the reason is that the Manabe and Stouffer model is unable to separate the Ekman layer associated with southeastwards flow from the underlying subtropical gyre associated with more westwards flow

in the Mururoa region. It would thus be a problem of vertical resolution. The above-mentioned averaging over the first five levels (50 m) is assumed to produce a flow close to that computed with a lower vertical resolution, and is still rather eastwards in the vicinity of Mururoa. In other words, when our model's Ekman layer currents are averaged with the gyre currents, the flow is still oriented in a direction opposite to that found by RT. Therefore, we consider that our study better supports an explanation in terms of differences mainly in atmospheric surface forcing, which underscores the responsiveness of direction to those conditions. In contrast, changes in the maximum concentration with time are comparable, which tends to boost our confidence in the quantitative aspects of the results; the orders of magnitude of the concentrations, as determined by this study, are reliable. We believe that our study can help to evaluate the consequence of any passive tracer injection from Mururoa atoll into the Pacific Ocean.

Acknowledgements

The authors would like to thank Olivier Marti and Harilaos Loukos for their help and comments. Gratitude is expressed to Gurvan Madec and Pascale Delecluse for fruitful discussions.

References

Blanke, B., & Delecluse, P. (1993). Variability of the tropical Atlantic Ocean simulated by a general circulation model with two different mixed-layer physics. *Journal of Physical Oceanography*, *23*, 1363–1388.

Delecluse, P., Madec, G., Imbard, M., & Levy, C. (1993). OPA version 7 ocean circulation model reference manual. Internal report LODYC 93/05, 111 pp.

Esbensen, S.K., & Kushnir, Y. (1981). The heat budget of the global ocean: an atlas based on estimates from marine surface observations. *Climatic Research Institute*, Oregon State Univ., Corvallis, Rep. 29, 27 pp.

Guilyardi E., & Madec, G. (1997). Performance of the OPA/ARPEGE-T21 global ocean–atmosphere coupled model. *Climate Dynamics*, *13*, 149–165.

Hellerman, S., & Rosenstein, M. (1983). Normal monthly wind stress over the world ocean with error estimates. *Journal of Physical Oceanography*, *13*, 1093–1104.

Levitus, S. (1982). Climatological atlas of the world ocean. *NOAA professional paper*, 13, 173 pp.

Madec, G., & Imbard, M. (1996). A global ocean mesh to overcome the north pole singularity. *Climate Dynamics*, *12*, 381–388.

Manabe, S., & Stouffer, R. J. (1988). Two stable equilibria of a coupled ocean–atmosphere model. *Journal of Climate*, *1*(9), 841–866.

Marti, O. (1992). Etude de l"océan mondial: modélisation de la circulation et du transport des traceurs anthropiques. Thesis of University Paris VI.

Oberhuber, J. M. (1988). An atlas based on the 'COADS' data set: the budget of heat, buoyancy and turbulent kinetic energy at the surface of the global ocean. *Max Planck Institut Report*, *15*, 20 pp.

Orr, J.C. (1993). Accord between ocean models predicting uptake of anthropogenic CO_2. *Water, Air and Soil Pollution*, *70*, 465–481.

Philander, S. G. H. (1990). El Niño, La Niña, and the Southern Oscillation. *International Geophysics Series*, *46*.

Reverdin, G., Frankignoul, C., Kestenare, E., & McPhaden, M. J. (1994). Seasonal variability in the surface currents of the equatorial Pacific. *Journal of Geophysical Research*, *99*(C10), 20323–20344.

Ribbe, J., & Tomckzak, M. (1990). An Impact Assessment for the French Nuclear Sites in French Polynesia. *Marine Pollution Bulletin*, *21*(11), 536–542.

Smolarkiewicz, P. K., & Clark, T. L. (1986). The multidimensional positive definite advection transport algorithm: further development and applications. *Journal of Computational Physics*, *67*, 396–438.